Methods of Controlling Lift-off in Conductivity Invariance Phenomenon for Eddy Current Testing

Zhongwen Jin, Yuwei Meng, Rongdong Yu, Ruochen Huang[2,*], Mingyang Lu[2,*], Hanyang Xu[2], Xiaobai Meng[3], Qian Zhao[4], Zhijie Zhang[5], Anthony Peyton[2], Wuliang Yin[2*]

[1]Zhejiang Energy R&D Institute, Hangzhou, Zhejiang, 310003 China
[2]School of Electrical and Electronic Engineering, University of Manchester, Manchester, M13 9PL UK
[3]Faculty of Art, Science and Technology, University of Northampton, Northampton, NN2 6JD UK
[4]College of Engineering, Qufu Normal University, Shandong, 273165 China
[5]School of Instrument and Electronics, North University of China, Taiyuan, Shanxi, 030051 China

*Corresponding author:

Ruochen Huang (ruochen.huang@manchester.ac.uk);

Mingyang Lu (mingyang.lu@manchester.ac.uk);

Wuliang Yin (wuliang.yin@manchester.ac.uk)

ABSTRACT Previously, a conductivity invariance phenomena (CIP) has been discovered – at a certain lift-off, the inductance change of the sensor due to a test sample is immune to conductivity variations, i.e. the inductance – lift-off curve passes through a common point at a certain lift-off, termed as conductivity invariance lift-off. However, this conductivity invariance lift-off is fixed for a particular sensor setup, which is not convenient for various sample conditions. In this paper, we propose using two parameters in the coil design – the horizontal and vertical distances between the transmitter and the receiver to control the conductivity invariance lift-off. The relationship between these two parameters and the conductivity invariance lift-off is investigated by simulation and experiments and it has been found that there is an approximate linear relationship between these two parameters and the conductivity invariance lift-off. This is useful for applications where the measurements have restrictions on lift-off, e.g. uneven coating thickness which limits the range of the lift-off of probe during the measurements. Therefore, based on this relationship, it can be easier to adjust the configuration of the probe for a better inspection of the test samples.

INDEX TERMS Conductivity Invariance Phenomenon, Conductivity invariance lift-off, Sensor design, Eddy current testing, Electrical conductivity, Non-destructive testing

I. INTRODUCTION

In recent decades, non-destructive testing (NDT) has been widely used. Eddy current testing (ECT), as one of the most universal NDT techniques, has extensive applications for thickness measurement, the inspection of material integrity (e.g. crack detection) and the evaluation of material properties (e.g. electrical conductivity and magnetic permeability) [1]-[7]. However, the testing is significantly influenced by the material properties, lift-off and sensor structure, etc. As a result, various researches have been carried out to tackle this issue in pursuit of a better inspection of the test sample [8]-[16].

A precise estimation of the electrical conductivity and the magnetic permeability of the test sample is essential in many applications. Halleux et al. developed an equivalent simplified physical model for the electrical conductivity measurement and it can be applied in a wide range of metallic samples [17]. Moreover, a robust method by using frequency-dependent eddy current measurements was presented by Moulder et al. to determine the electrical conductivity of the uniform conductive layers [18]. Conductivity profiling from inductance spectroscopic measurements [19] and the conductivity measuring instrument for semi-conductors [20] also have been explored.

In terms of permeability measurements, it is still challenging to determine the permeability of the material due to the influence of the environment condition and the material conductivity on the response signal. A novel method that can measure the conductivity and permeability of the metal samples simultaneously was proposed by Ma et al [21]. The conductivity can be obtained by the impedance change of the signal while the permeability can be measured by utilising the imaginary part of the signal. The results were proved to be accurate but the frequency range is limited for estimating the permeability. Yu et al. proposed the CIP and developed a device to determine the permeability by decoupling the influence of the conductivity and permeability [22]-[23]. In

addition, a novel algorithm to compensate the zero-crossing frequency point caused by the lift-off effect was proposed by Lu et al. and the error caused by the lift-off can be reduced to 7.5% [24]-[25]. Moreover, for the thick coating, the lift-off effect in PEC can be reduced by using the reference signals and normalization process [26] and it is found that the sensitivity of the sensor coil would be boosted with higher lift-off under a certain range of the coil gap [27].
In our previous work, measurement of permeability for ferrite metallic plates based on CIP was introduced and proved to work well [28]. Further, in this paper, we proposed using two parameters in the coil design – the horizontal and vertical distances between the transmitter and the receiver to control the conductivity invariance lift-off in order to make it more flexible in ECT where the measurements have restrictions on lift-off, e.g. uneven coating thickness and varying coating thickness which limit the range of the lift-off of probe during the measurements.

II. SENSOR PARAMETERS FOR CONTROLLING CIP LIFT-OFF

In order to investigate the conductivity invariance phenomenon, the arrangement of the excitation coil and the receiving coil should be non-axial to the test samples (showed in Fig. 1), otherwise, there is no conductivity invariance lift-off point from measurements.

For a particular non-axial sensor setup, the lift-off point of CIP is fixed. In this paper, we introduce two parameters, that is, the horizontal distance (w) and vertical distance (g) between the transmitter and the receiver to control the CIP lift-off. Two sensor setups are used for the investigation of how these two parameters affect the CIP lift-off, named as, Sensor A and Sensor B. Fig. 1 (a) depicts the configuration where the transmitter and receiver are placed in the same vertical level, while Fig. 1 (b) presents the case where the receiver is vertically lifted by a distance of g. By adjusting the value of these two parameters, the value of the lift-off of CIP would change accordingly. Hence, it is more beneficial for the permeability measurement that has a limited range of lift-off.

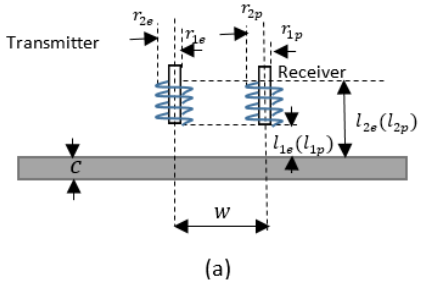

(a)

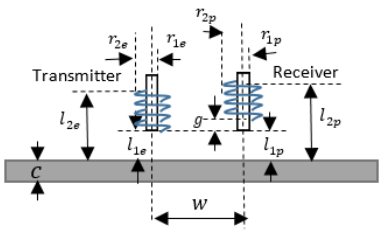

(b)

FIGURE 1. Sensor Geometry (a) Sensor A, transmitter and receiver are assembled in the same plane (b) Sensor B, receiver is vertically lifted with respect to the transmitter.

III. ANALYTICAL SOLUTION ON CIP LIFT-OFF

The complex inductance of an air-cored cylindrical coil caused by the metallic plate has been proposed by Dodd and Deeds for decades to offer strong interpretations of the electromagnetic phenomenon. Based on the formula of Dodd and Deeds analytical solution, the vector potentials from the excitation coil caused by the sample plate can be expressed as,

$$A(r,z) = \frac{\mu_0 I N_1}{(r_{2e}-r_{1e})(l_{2e}-l_{1e})} \int_0^\infty \frac{1}{\alpha^3} I(r_{2e}, r_{1e}) J_1(\alpha r)[2 - e^{\alpha(z-l_{2e})} - e^{\alpha(z-l_{1e})} + e^{-\alpha z}(e^{-\alpha l_{1e}} - e^{-\alpha l_{2e}}) \times \frac{(\alpha_1+\mu\alpha)(\alpha_1-\mu\alpha)-(\alpha_1+\mu\alpha)(\alpha_1-\mu\alpha)e^{2\alpha_1 c}}{-(\alpha_1-\mu\alpha)(\alpha_1-\mu\alpha)+(\alpha_1+\mu\alpha)(\alpha_1+\mu\alpha)e^{2\alpha_1 c}}]d\alpha \quad (1)$$

$$\alpha_1 = \sqrt{\alpha^2 + j\omega\sigma\mu\mu_0} \quad (2)$$

Where: μ_0 denotes the permeability of the free space, σ and μ denote the electrical conductivity and permeability of the sample plate, α denotes the spatial frequency variable, I denotes the excitation current flows in the coil, N_1 denotes the number of turns of the excitation coil, r_{1e} and r_{2e} denote the inner radius and the outer radius of the excitation coil, l_{1e} and l_{2e} denote the bottom height and top height of the excitation coil, $J_1(x)$ denotes the first order of the first kind of Bessel function and $I(x_1,x_2)$ denotes the production of , $J_1(x)$ from x_1 to x_2.
Furthermore, the voltage induced by a single loop of the receiving coil (Fig. 2) can be expressed as an integration of the vector potential over the cross-section of the coil.

$$V = jw \int A(r,z)ds = jw \int A(r,z) r_p cos\varphi d\theta \quad (3)$$

$$\varphi = \theta + tan^{-1}\left(\frac{r_p sin\theta}{w - r_p cos\theta}\right) \quad (4)$$

$$r = \sqrt{(r_p sin\theta)^2 + (w - r_p cos\theta)^2 + g^2} \quad (5)$$

Where: φ denotes the angle between the vector potential A and ds, r denotes the distance between the origin O and ds, g denotes the height difference between the excitation coil and receiving coil.

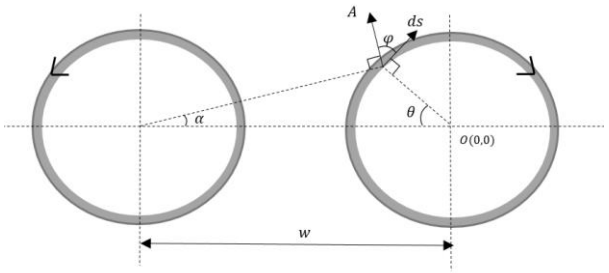

FIGURE 2. **Top view of sensor coils**

The voltage received in the receiving coil can be derived by combining (1)-(5). Two situations of sensor arrangement are considered, as shown in Fig. 1 (a) and (b). Hence the voltage induced can be expressed as (6) for Fig. 1(a) and (7) for Fig. 1(b).

$$V_a = \frac{jw\mu_0 IN_1N_2}{(r_{2e}-r_{1e})(l_{2e}-l_{1e})(r_{2p}-r_{1p})(l_{2p}-l_{1p})}\int_0^{\infty}\int_0^{2\pi}\int_{r_{1p}}^{r_{2p}}\cos\left(\theta + tan^{-1}\left(\frac{r_p sin\theta}{w-r_p cos\theta}\right)\right)\frac{1}{\alpha^3}I(r_{2e},r_{1e})J\left(\alpha\sqrt{(r_p sin\theta)^2+(w-r_p cos\theta)^2}\right)\left(2(l_{2e}-l_{1e})-\frac{1}{\alpha}[2e^{-\alpha(l_{2e}-l_{1e})}-2+(e^{-\alpha l_{1e}}-e^{-\alpha l_{2e}})^2\frac{(\alpha_1+\mu\alpha)(\alpha_1-\mu\alpha)-(\alpha_1+\mu\alpha)(\alpha_1-\mu\alpha)e^{2\alpha_1 c}}{-(\alpha_1-\mu\alpha)(\alpha_1-\mu\alpha)+(\alpha_1+\mu\alpha)(\alpha_1+\mu\alpha)e^{2\alpha_1 c}}]\right)dr_p d\theta d\alpha \quad (6)$$

$$V_b = \frac{jw\mu_0 IN_1N_2}{(r_{2e}-r_{1e})(l_{2e}-l_{1e})(r_{2p}-r_{1p})(l_{2p}-l_{1p})}\int_0^{\infty}\int_0^{2\pi}\int_{r_{1p}}^{r_{2p}}\cos\left(\theta + tan^{-1}\left(\frac{r_p sin\theta}{w-r_p cos\theta}\right)\right)\frac{1}{\alpha^3}I(r_{2e},r_{1e})J\left(\alpha\sqrt{(r_p sin\theta)^2+(w-r_p cos\theta)^2+g^2}\right)\left(2(l_{2p}-l_{1p})-\frac{1}{\alpha}[e^{-\alpha(l_{2p}-l_{2e})}-e^{-\alpha(l_{1p}-l_{2e})}+e^{-\alpha(l_{2p}-l_{1e})}-e^{-\alpha(l_{1p}-l_{1e})}+(e^{-\alpha l_{2p}}-e^{-\alpha l_{1p}})(e^{-\alpha l_{1e}}-e^{-\alpha l_{2e}})\frac{(\alpha_1+\mu\alpha)(\alpha_1-\mu\alpha)-(\alpha_1+\mu\alpha)(\alpha_1-\mu\alpha)e^{2\alpha_1 c}}{-(\alpha_1-\mu\alpha)(\alpha_1-\mu\alpha)+(\alpha_1+\mu\alpha)(\alpha_1+\mu\alpha)e^{2\alpha_1 c}}]\right)dr_p d\theta d\alpha \quad (7)$$

Where: N_2 denotes the number of turns of the sensing coil, r_{1p} and r_{2p} denote the inner radius and the outer radius of the sensing coil, l_{1p} and l_{2p} denote the bottom height and top height of the sensing coil.

With further manipulations from (6) and (7), the complex mutual inductance between the excitation coil and the receiving coil can be derived as (8) for Fig. 1(a) and (9) for Fig. 1(b).

$$L_a = \frac{\mu_0 N_1N_2}{(r_{2e}-r_{1e})(l_{2e}-l_{1e})(r_{2p}-r_{1p})(l_{2p}-l_{1p})}\int_0^{\infty}\int_0^{2\pi}\int_{r_{1p}}^{r_{2p}}\cos\left(\theta + tan^{-1}\left(\frac{r_p sin\theta}{w-r_p cos\theta}\right)\right)\frac{1}{\alpha^3}I(r_{2e},r_{1e})J\left(\alpha\sqrt{(r_p sin\theta)^2+(w-r_p cos\theta)^2}\right)\left(2(l_{2e}-l_{1e})-\frac{1}{\alpha}[2e^{-\alpha(l_{2e}-l_{1e})}-2+(e^{-\alpha l_{1e}}-e^{-\alpha l_{2e}})^2\frac{(\alpha_1+\mu\alpha)(\alpha_1-\mu\alpha)-(\alpha_1+\mu\alpha)(\alpha_1-\mu\alpha)e^{2\alpha_1 c}}{-(\alpha_1-\mu\alpha)(\alpha_1-\mu\alpha)+(\alpha_1+\mu\alpha)(\alpha_1+\mu\alpha)e^{2\alpha_1 c}}]\right)dr_p d\theta d\alpha \quad (8)$$

$$L_b = \frac{\mu_0 N_1N_2}{(r_{2e}-r_{1e})(l_{2e}-l_{1e})(r_{2p}-r_{1p})(l_{2p}-l_{1p})}\int_0^{\infty}\int_0^{2\pi}\int_{r_{1p}}^{r_{2p}}\cos\left(\theta + tan^{-1}\left(\frac{r_p sin\theta}{w-r_p cos\theta}\right)\right)\frac{1}{\alpha^3}I(r_{2e},r_{1e})J\left(\alpha\sqrt{(r_p sin\theta)^2+(w-r_p cos\theta)^2+g^2}\right)\left(2(l_{2p}-l_{1p})-\frac{1}{\alpha}[e^{-\alpha(l_{2p}-l_{2e})}-e^{-\alpha(l_{1p}-l_{2e})}+e^{-\alpha(l_{2p}-l_{1e})}-e^{-\alpha(l_{1p}-l_{1e})}+(e^{-\alpha l_{2p}}-e^{-\alpha l_{1p}})(e^{-\alpha l_{1e}}-e^{-\alpha l_{2e}})\frac{(\alpha_1+\mu\alpha)(\alpha_1-\mu\alpha)-(\alpha_1+\mu\alpha)(\alpha_1-\mu\alpha)e^{2\alpha_1 c}}{-(\alpha_1-\mu\alpha)(\alpha_1-\mu\alpha)+(\alpha_1+\mu\alpha)(\alpha_1+\mu\alpha)e^{2\alpha_1 c}}]\right)dr_p d\theta d\alpha \quad (9)$$

Here, all the analytical solutions were calculated via the platform ThinkCenter M910s, with 16GB RAM and Intel Core i7-6700 processor.

IV. EXPERIMENTAL SETUP ON CIP LIFT-OFF

Due to the restriction in access such as coating thickness on the test sample, there exists a minimum lift-off during inspection. To address this issue, both simulation by analytical calculation and the experimental measurements have been carried out to verify the relationship between the horizontal and vertical distances of the sensor coils and the conductivity invariance lift-off point.

During the experimental measurements, the sensor shown in Fig. 3 was used to detect the feature of this phenomenon. The horizontal distance between two sensor coils was set to 3 mm, 4 mm and 5 mm respectively. The test samples have a length of 80 mm, a width of 80 mm and a thickness of 5 mm. Three types of materials were tested under the excitation frequency of 60 kHz, copper, aluminium and brass respectively. The conductivities of these materials are 57 MS/m, 35 MS/m, 16 MS/m at 20 degrees and the relative permeability is 1 for conductive materials. The experimental setup is showed in Fig. 3 and the sensor parameters are listed in Table 1.

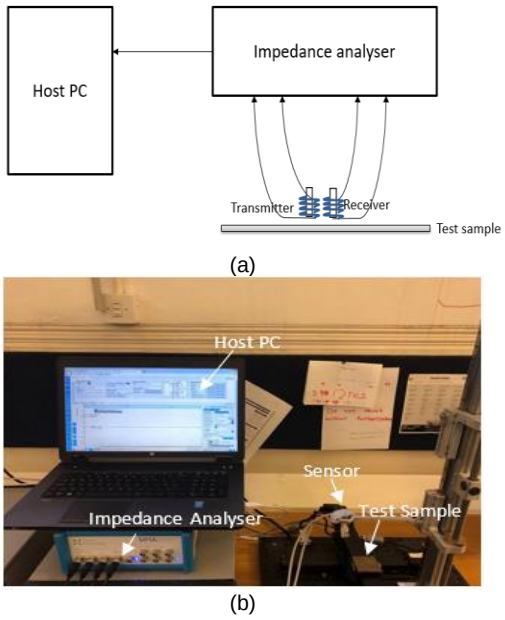

FIGURE 3. **Experimental Setup (a) schematic setup (b) actual setup**

TABLE I
SENSOR PARAMETERS

Inner and outer radii of the excitation coil (r_{1e} / r_{2e})	0.75 mm/0.95 mm
Inner and outer radii of the receiving coil (r_{1p} / r_{2p})	0.75 mm/1.10 mm
Height of the excitation coil (l_{2e}- l_{1e})	3 mm
Height of the receiving coil (l_{2p}- l_{1p})	3 mm
Turns of excitation coil and receiving coil (N_1 / N_2)	120/160
Plate thickness (c)	5 mm
The horizontal distance between two coils (w)	3 – 5 mm
The vertical distance between two coils (g)	-1 – 1 mm

From the schematic setup shown in Fig. 3(a), the injection current flows into the transmitter and can induces the voltage on the receiver, then the impedance between the transmitter and the receiver can be obtained via the impedance analyser. It is because there is a phase difference between the induced voltage and the excitation current, the tested impedance should be complex. Therefore, the complex inductance can be presented by dividing the mutual impedance by the excitation frequency in the experimental measurements, as shown in (10)-(13). Further, the inductance of one of the metal plates was set as a reference for the inductance of all the samples, the conductivity invariance lift-off can be found by the inductance changes with respect to the reference inductance. It is worth noting that the real part of the inductance change is mainly due to the change of the magnetic flux affected by the metallic plate, meanwhile, the loss mainly due to the eddy current effect reflects on the change of the imaginary part of the inductance.

$$Z = R + j\omega L \tag{10}$$

$$\Delta L = \frac{\Delta Z}{j\omega} \tag{11}$$

$$\mathrm{Re}(\Delta \mathrm{L}) = \mathrm{Re}\left(\frac{Z_{sample} - Z_{air}}{j\omega}\right) \tag{12}$$

$$\mathrm{Im}(\Delta \mathrm{L}) = \mathrm{Im}\left(\frac{Z_{sample} - Z_{air}}{j\omega}\right) \tag{13}$$

Where: Z_{sample} denotes the impedance caused by the metallic sample plate and Z_{air} denotes the impedance in the air.

V. RESULTS

A. VALIDATION OF CIP LIFT-OFF

Through experimental results and simulation results shown in Fig. 4, there exists the conductivity invariance lift-off for the non-magnetic conductive / ferromagnetic materials. The maximum error between the experiments and simulations for varying lift-off is 7.46% for Fig. 4 (a). However, at the conductivity invariance lift-off point, the error of the inductance variation can be neglected since it is controlled within a relatively small range of 0.1%. Therefore, it is an ideal sensor position for material inspection under different configurations of the sensor. For permeability measurements with the material in which the conductivities are known, assume all the materials with the same permeability, the conductivity invariance lift-off can be obtained from the simulation, as shown in Fig. 4(b). Compared with the results from Fig. 4(a), the conductivity invariance lift-off decreases as the relative permeability increases. Thus, from the experimental measurements under this conductivity invariance lift-off, the permeability can be predicted from the offset of the curves.

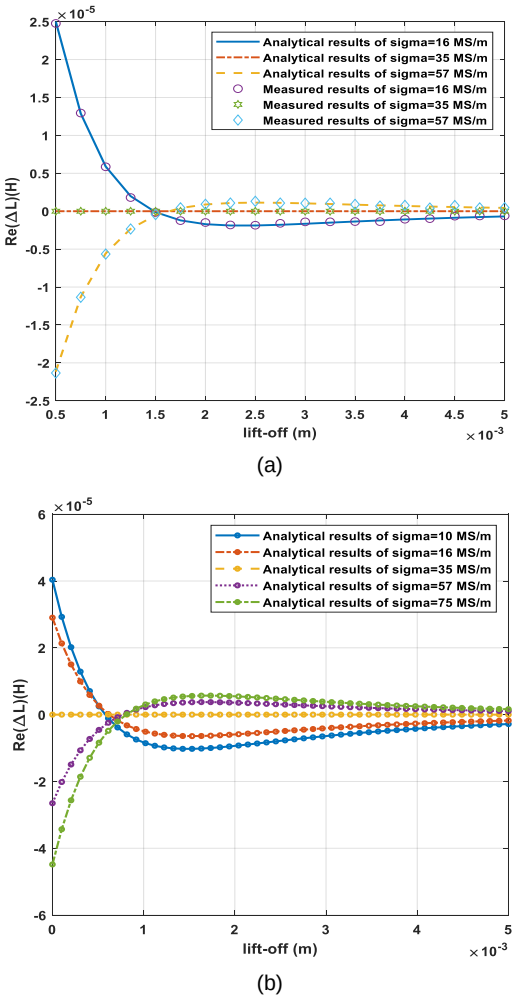

FIGURE 4. CIP validation (a) Results of conductive materials ($\mu_r = 1$) (b) Analytical solution of ferromagnetic materials under ($\mu_r = 300$)

B. CIP LIFT-OFF EVALUATION

To investigate the relationship between the horizontal/vertical distance of the transmitter and the receiver and the CIP, analytical simulation and experiments have been carried out. A linear relationship has been found between the horizontal/vertical distance of the transmitter and the receiver and the CIP, as shown in the following Fig. 5 and 6.

B.1. Horizontal distance

In this section, sensor A (showed in Fig. 1(a)) was used to investigate how the relationship between the horizontal distance and the conductivity invariance lift-off changes. Table II illustrates the error between the simulated results and the measured results. The error between them can be achieved within 1.5%. More horizontal distances (in steps of 0.25 mm) have been considered by utilizing the analytical solution and the results are shown in Fig. 5. The dashed line

shows the trend of the change of conductivity invariance lift-off. As the horizontal distance increase, the lift-off increases to observe the predominant magnetic flux passing through the receiver regardless of the sample conductivities. It can be noticed that there is an approximated linear relationship between the horizontal distance of sensor coils and the conductivity invariance lift-off.

TABLE II
SIMULATED AND MEASURED CONDUCTIVITY INVARIANCE LIFT-OFF POINTS UNDER DIFFERENT HORIZONTAL DISTANCE

Horizontal distance between two sensor coils (w)	Simulated conductivity invariance lift-off (m)	Measured conductivity invariance lift-off (m)	Error (%)
3 mm	1.51e-3	1.53e-3	1.32
4 mm	2.56e-3	2.57e-3	0.39
5 mm	3.67e-3	3.70e-3	0.82

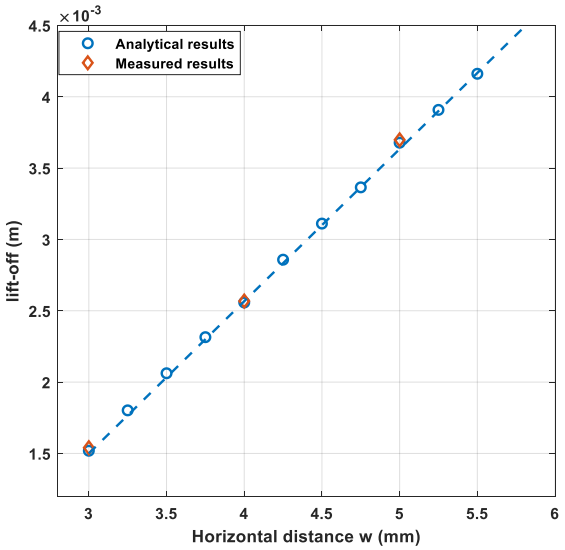

FIGURE 5. The analytical and measured results of the conductivity invariance lift-off under different horizontal distances between the sensor coils from sensor A

B.2. Vertical distance

As shown in Fig. 1(b), sensor B was used to investigate how the conductivity invariance lift-off changes with the vertical distance. For experimental measurements, the vertical distance between the excitation coil and the sensing coil was set to -0.5 mm (the receiver is 0.5 mm lower than the transmitter), 0 mm, and 0.5 mm (the receiver is 0.5 mm higher than the transmitter) respectively while the horizontal distance was kept to 3 mm. The analytical solution was used to simulate more possible vertical distance to evaluate the relations (the vertical distance changes from -1 mm to 1 mm in steps of 0.25 mm). The results are presented in Fig. 6. The trends of the results are matched with the trend lines (dashed lines). Table III depicts the conductivity invariance lift-off between simulation and measurements and the error is within 3%. It can be seen from Fig. 6 that there is a decreasing trend as the receiver move from the bottom up with respect to the transmitter. Thus, there is a trade-off for researchers to select the configurations for the sensor through these relations to match their measurement conditions.

TABLE III
SIMULATED AND MEASURED CONDUCTIVITY INVARIANCE LIFT-OFF POINTS UNDER DIFFERENT VERTICAL DISTANCE

Vertical distance between two sensor coils (g)	Simulated conductivity invariance lift-off (m)	Measured conductivity invariance lift-off (m)	Error (%)
-0.5 mm	1.69e-3	1.66e-3	-1.78
0 mm	1.49e-3	1.53e-3	2.68
0.5 mm	1.25e-3	1.23e-3	-1.60

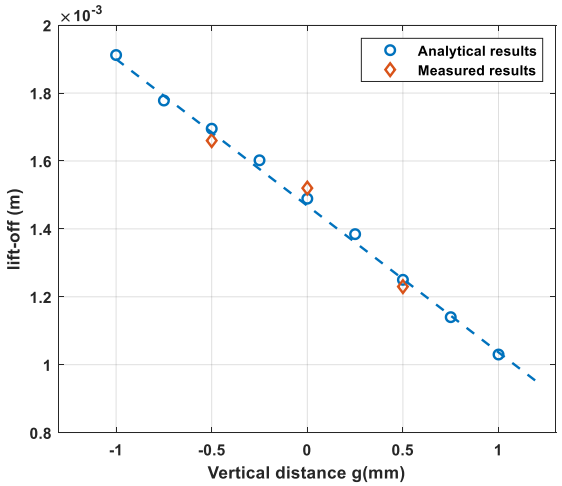

FIGURE 6. The analytical results of the conductivity invariance lift-off point under different vertical distances and fixed horizontal distance w of 3 mm

VI. DISCUSSIONS

A. EFFECT OF SAMPLE THICKNESS

The thickness of the samples has an influence on the conductivity invariance lift-off. In the numerical simulation, sensor A was used, and the sample thicknesses are 0.05 mm, 1 mm, 5 mm and 15 mm respectively. All the samples were simulated under the excitation frequency of 60 kHz. Conductivity invariance lift-off for different sample thicknesses goes along with the dashed lines showed in Fig. 8. It is found that there is no conductivity invariance lift-off as the sample thickness was 0.05 mm (Fig. 7) while the conductivity invariance lift-off does not increase any more as the sample thickness reaches a certain amount (Fig. 8). The reason that there is no conductivity invariance lift-off is that the skin depth is larger than the thickness of the samples so that most of the magnetic flux penetrates through the samples, which could influence the vector potential to be integrated on the cross-section of the sensing coil (i.e. the

induced voltage) as the sensor moving vertically. As the sample thickness increases to a certain range, the skin depth is smaller than the sample thickness, all the magnetic flux would be reflected by the test samples and the induced voltage on the sensor coil. Therefore, the conductivity invariance lift-off stays at a similar value. It can be seen in Fig. 8 that the conductivity invariance lift-off decreases as the sample becomes thicker while for the arbitrary thickness of the test samples, there is a linear trend between the conductivity invariance lift-off and the horizontal distance of the sensor coils.

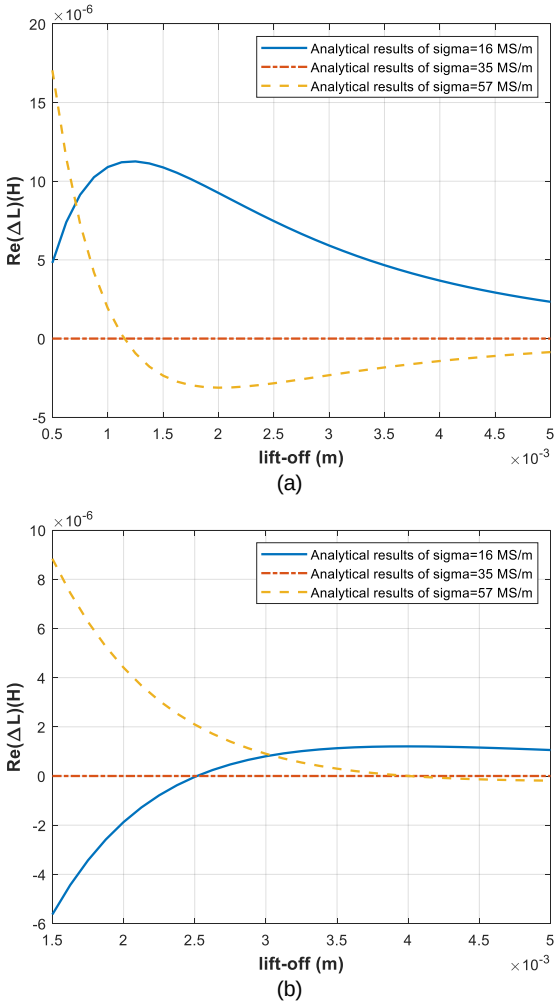

FIGURE 7. Analytical solution of the sample thickness 0.05 mm under different widths between the sensor coils (a) 3 mm (b) 5 mm

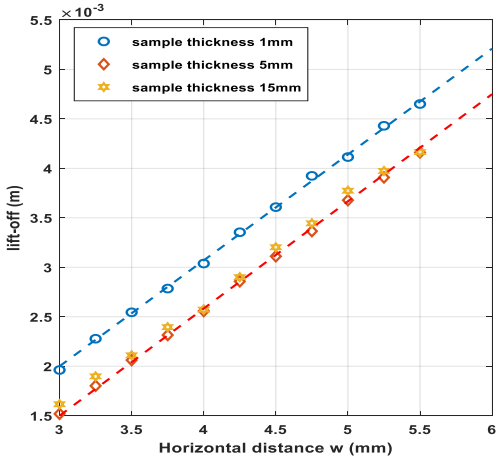

FIGURE 8. Conductivity invariance lift-off under different horizontal distances between the sensor coils and sample thicknesses

B. EFFECT OF DIFFERENT FREQUENCIES

Fig. 9 demonstrates the simulation results of the conductivity invariance lift-off under two excitation frequencies: 50 kHz and 500 kHz. During the simulation, the thickness of the test samples is set to be 1 mm and sensor A was used. As shown in Fig. 9, with a fixed sensor setup, a higher excitation frequency will lead to an increase of the conductivity invariance lift-off, which is due to the skin depth effect. For different frequencies, the lift-off increase linearly with the increase of the width, as shown by the dashed line (trend line). Additionally, it can be noticed that, as the horizontal distance between two coils gradually increases, the changes of the lift-off from the results under the frequency of 500 kHz is slightly larger than that under 50 kHz.

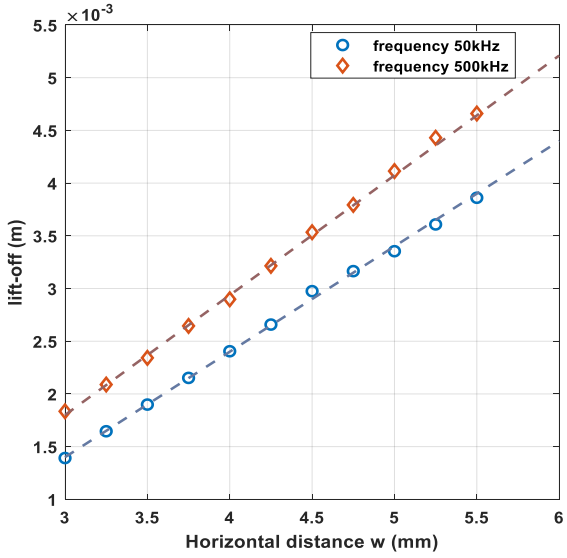

FIGURE 9. Analytical solutions of conductivity invariance lift-off under different horizontal distances between the sensor coils and excitation frequencies

VII. CONCLUSIONS

In this paper, the impact of changing horizontal and vertical distance between the transmitter coil and the receiver coil on the conductivity invariance lift-off was investigated. It is found that there is a good linear relationship between them for materials of different electrical conductivities. Both the analytical and measured results have verified this relationship.

Based on this feature, the conductivity invariance lift-off can be adjusted for cases where there is restriction of access to the test sample. Moreover, the effect of the sample thickness and the excitation frequency on the relations are all discussed, and it proves that linear relation is always valid for these factors.

ACKNOWLEDGEMENT

This work was supported by [UK Engineering and Physical Sciences Research Council (EPSRC)] [grant number: EP/P027237/1] [title: Real-time In-line Microstructural Engineering (RIME)].

REFERENCES

[1] G. Y. Tian, A. Sophian, D. Taylor, and J. Rudlin, “Multiple sensors on pulsed eddy-current detection for 3-D subsurface crack assessment,” IEEE Sensors J., vol. 5, no. 1, pp. 90–96, Feb. 2005.

[2] C. Ye, Y. Huang, L. Udpa, S. Udpa, and A. Tamburrino, “Magnetoresistive sensor with magnetic balance measurement for inspection of defects under magnetically permeable fasteners,” IEEE Sensors J., vol. 16, no. 8, pp. 2331–2338, Apr. 2016.

[3] J. R. S. Avila, K. Y. How, M. Lu, and W. Yin, “A novel dual modality sensor with sensitivities to permittivity, conductivity, and permeability,” IEEE Sensors J., vol. 18, no. 1, pp. 356–362, Jan. 2018.

[4] W. Yin, A. J. Peyton and S. J. Dickinson, “Simultaneous measurement of distance and thickness of a thin metal plate with an electromagnetic sensor using a simplified model,” IEEE Transactions on Instrumentation and Measurement, vol. 53, no. 4, pp. 1335–1338, Aug. 2004.

[5] X. Ma, A.J. Peyton and Y. Zhao. “Measurement of the electrical conductivity of open-celled aluminium foam using non-contact eddy current techniques,” NDT & E International, vol. 38, pp. 359-397, 2005.

[6] B. Ye, J. Cai, P. Huang, M. Fan and Z. Zhou, “Automatic Recognition and Classification of Eddy Current Testing Signals for Scanning Inspection of Defect in Multi-layered Structure,” Chinese Journal of Sensors and Actuators, vol. 20, no. 10. Pp. 2253-2258, Oct. 2007.

[7] M. Lu, X. Meng, W. Yin, Z. Qu, et al. “Thickness measurement of non-magnetic steel plates using a novel planar triple-coil sensor,” NDT & E International, vol. 107, Oct. 2019.

[8] W Yin, XJ Hao, AJ Peyton, M Strangwood and CL Davis. “Measurement of permeability and ferrite/austenite phase fraction using a multi-frequency electromagnetic sensor,” NDT & E International, vol. 42, no. 1, pp. 64-68, 2009.

[9] I. D. Adewale and G. Y. Tian, "Decoupling the Influence of Permeability and Conductivity in Pulsed Eddy-Current Measurements," IEEE Transactions on Magnetics, vol. 49, no. 3, pp. 1119-1127, Mar. 2013.

[10] X. Ma and A. J. Peyton, "Eddy current measurement of the electrical conductivity and porosity of metal foams," IEEE Transactions on Instrumentation and Measurement, vol. 55, no. 2, pp. 570-576, Apr. 2006.

[11] X. Chen and Y. Lei, “Electrical conductivity measurement of ferromagnetic metallic materials using pulsed eddy current method,” NDT & E International, vol. 75, pp. 33-38, Oct. 2015.

[12] W. Yin and K. Xu, "A Novel Triple-Coil Electromagnetic Sensor for Thickness Measurement Immune to Lift-Off Variations," IEEE Transactions on Instrumentation and Measurement, vol. 65, no. 1, pp. 164-169, Jan. 2016.

[13] S. Li, S. Huang and W. Zhao, “Development of differential probes in pulsed eddy current testing for noise suppression,” Sensors and Actuators A: Physical, vol. 135, no. 2, pp. 675-679, Apr. 2007.

[14] H. Hoshikawa, K. Koyama and H. Karasawa, “A new eddy current surface probe without lift-off noise,” AIP Conference Proceedings, vol. 557, no. 1, pp. 969-976, Jan. 2001.

[15] C. Wang, M. Fan, B. Cao, B. Ye, W. Li, “Novel Noncontact Eddy Current Measurement of Electrical Conductivity,” IEEE Sensors Journal, vol. 18, no. 22, pp. 9352-9359, Nov. 2018.

[16] D. Wen, M. Fan, B. Cao, B. Ye, and G. Tian, “Extraction of LOI Features From Spectral Pulsed Eddy Current Signals for Evaluation of Ferromagnetic Samples,” IEEE Sensors Journal, vol. 19, no. 1, pp. 189-195, Oct. 2018.

[17] Benoit de Halleux, Bruno de Limburg Stirum and Andrei I'tchelintsev, “Eddy current measurement of the wall thickness and conductivity of circular non-magnetic conductive tubes,” NDT & E International, vol. 29, no. 2, pp. 103-109, Apr. 1996.

[18] John C. Moulder, Erol Uzal, and James H. Rose, “Thickness and conductivity of metallic layers from eddy current measurements,” Review of Scientific Instruments, vol. 63, no. 6, pp. 3455-3465, Jan. 1992.

[19] W. Yin, S. J. Dickinson, and A. J. Peyton, “Imaging the continuous conductivity profile within layered metal structures using inductance spectroscopy,” IEEE Sensors J., vol. 5, no. 2, pp. 161–166, Apr. 2005.

[20] F. Loete, Y. Le Bihan and D. Mencaraglia, "Novel Wideband Eddy Current Device for the Conductivity Measurement of Semiconductors," IEEE Sensors Journal, vol. 16, no. 11, pp. 4151-4152, June, 2016.

[21] X. Ma, A.J. Peyton and Y.Y. Zhao, “Eddy current measurements of electrical conductivity and magnetic permeability of porous metals,” NDT & E International, vol. 39, no. 7, pp. 562-568, Oct. 2006.

[22] Y. Yu, Y. Zou, M. A. Hosani and G. Tian, "Conductivity Invariance Phenomenon of Eddy Current NDT: Investigation, Verification, and Application," IEEE Transactions on Magnetics, vol. 53, no. 1, pp. 1-7, Jan. 2017.

[23] Y. Yu, Y. Zou, M. Jiang and D. Zhang, "Investigation on conductivity invariance in eddy current NDT and its application on magnetic permeability measurement," 2015 IEEE Far East NDT New Technology & Application Forum (FENDT), pp. 257-262, 2015.

[24] M. Lu, W. Zhu, L. Yin, A. J. Peyton, W. Yin and Z. Qu, "Reducing the Lift-Off Effect on Permeability Measurement for Magnetic Plates From Multifrequency Induction Data," IEEE Transactions on Instrumentation and Measurement, vol. 67, no. 1, pp. 167-174, Jan. 2018.

[25] M. Lu, R. Huang, W. Yin, Q. Zhao and A. Peyton, "Measurement of Permeability for Ferrous Metallic Plates Using a Novel Lift-Off Compensation Technique on Phase Signature," IEEE Sensors Journal, vol. 19, no. 17, pp. 7440-7446, 1 Sept.1, 2019.

[26] G. Y. Tian and A. Sophian, “Reduction of lift-off effects for pulsed eddy current NDT,” NDT E Int., vol. 38, no. 4, pp. 319–324, 2005.

[27] D. I. Ona, G. Y. Tian, R. Sutthaweekul and S. M. Naqvi, “Design and optimisation of mutual inductance based pulsed eddy current probe”, Measurement 144, vol. 144, pp. 402-409, Oct. 2019.

[28] M. Lu, H. Xu, W. Zhu, L. Yin et al. “Conductivity Lift-off Invariance and measurement of permeability for ferrite metallic plates,” NDT & E International, vol. 95, pp. 36-44, Apr. 2018.